

## Article

# Variations in Temperature and Pressure in the “Reservoir–Well” System Triggered by Blasting Recovery of Iron Ore at the Kursk Magnetic Anomaly

Ella Gorburnova <sup>\*</sup>, Sofia Petukhova , Aleksey Ivanov , Zulfat Sharafiev , Dmitry Pavlov , Artem Karavaev and Andrey Fedorov

Deformation Processes in the Earth’s Crust, Sadovsky Institute of Geospheres Dynamics of Russian Academy of Sciences, Moscow 119334, Russia; petukhova.sm@idg.ras.ru (S.P.); ivanov.ag@idg.ras.ru (A.I.); sharafiev.zz@idg.ras.ru (Z.S.); pavlov.dv@idg.ras.ru (D.P.); karavaev.av@idg.ras.ru (A.K.); fedorov.ayu@idg.ras.ru (A.F.)

\* Correspondence: emgorburnova@bk.ru

**Abstract:** This paper presents the results of precise measurements of temperature and pore pressure in the “reservoir–well” system during the development of iron ore deposits of the Kursk Magnetic Anomaly (KMA) via blasting. For the observation period from October 2021 to June 2024, variations in compressibility, permeability and temperature in the upper Albian–Cenomanian confined aquifer, which is used for district water supply, were determined. The general trend in a decrease in water temperature was traced (from 12 °C to 11.4 °C). It was accompanied by an increase in the hydrostatic head (from 3.7 m to 7.4 m). Water temperature in the upper aquifer was measured for 9 industrial explosions in the mine and for 30 explosions in the quarry. For one explosion in the mine and five explosions in the quarry the coseismic changes in water temperature with amplitudes of 0.06–0.09 °C were established, while changes in pore pressure in the “reservoir–well” system were 0.4–2.2 kPa. Local changes in the permeability of the reservoir in the vicinity of the well (the skin effect) are considered to be the main factor that controls the coseismic response of temperature during industrial explosions. As the reservoir permeability increases, the water temperature in the “reservoir–well” system can decrease and vice versa. The same pattern was observed according to regime measurements performed in 2022–2023. The recorded coseismic responses of water temperature in the upper aquifer in the high-frequency range are similar to the effects observed during propagation of seismic waves originated from earthquakes in the low-frequency range at different sites all over the world for the seismic energy density of 0.05–0.45 J/m<sup>3</sup>. The observed variations in aquifer temperature in the “reservoir–well” system under episodic dynamic impacts are of particular interest from the point of view of activating hydrogeochemical processes that accompany the development of iron ore deposits.

**Keywords:** precision hydrogeological monitoring; temperature in aquifer; industrial explosions; “reservoir–well” system; permeability; coseismic effects



**Citation:** Gorburnova, E.; Petukhova, S.; Ivanov, A.; Sharafiev, Z.; Pavlov, D.; Karavaev, A.; Fedorov, A. Variations in Temperature and Pressure in the “Reservoir–Well” System Triggered by Blasting Recovery of Iron Ore at the Kursk Magnetic Anomaly. *Water* **2024**, *16*, 2682. <https://doi.org/10.3390/w16182682>

Received: 28 August 2024

Revised: 15 September 2024

Accepted: 18 September 2024

Published: 20 September 2024



**Copyright:** © 2024 by the authors. Licensee MDPI, Basel, Switzerland. This article is an open access article distributed under the terms and conditions of the Creative Commons Attribution (CC BY) license (<https://creativecommons.org/licenses/by/4.0/>).

## 1. Introduction

Modern precision sensors allow registering not only quasistatic variations in the water level and temperature in water-bearing layers, but fast dynamic variations under episodic impacts as well, which facilitates noticeably current hydrogeologic investigations. The temperature of rock and water can be considered as indicators of hydrogeologic changes, emergence of cross-flows, and local changes in the filtration properties of the “reservoir–well” system.

An annual cyclicity of bedrock temperature has been observed in natural conditions inside the Chinese Platform according to the monitoring data obtained in a well 12 m deep, which tapped shales located in the damage zone of the regional fault Xianshuihe [1]. The

amplitude of seasonal variations in rock temperature decreased from 2.3 °C at a depth of 5.9 m to 0.8 °C at a depth of 10.1 m. The annual maximum of rock temperature occurred with a time lag of up to 3 months as the depth of observations changed by 4.2 m. Daily variations in the temperature of water-bearing rocks with amplitudes of 0.002–0.006 °C were detected in the raw data at a depth of 5.9 m. The earthquake Kangding M 6.3 22 November 2014 that occurred in the Sichuan province, China was accompanied by the following events in the same well [1]: a coseismic stepwise rise in rock temperature by 0.01 °C at a depth of 9.0 m; a gradual post-seismic decrease in temperature by 0.0002 °C in the depth interval of 1–7 m.

Similar differently directed water temperature variations were registered in different observation points during propagation of waves produced by earthquakes [2]. For example, stepwise coseismic rise in the water level, discharge and temperature increase during 14 earthquakes M 4.2–9.2 at epicentral distances of 4–3076 km were observed for the period of 2004–2015 in the well Dazhai in south-west China. The well is 112 m deep. It tapped a confined aquifer in siltstones and sandstones [3]. Variations in amplitudes of the registered parameters were as follows: water level—from 58 to 410 mm; discharge—from 0.01 to 0.2 L/s; temperature—from 0.005 to 0.4 °C.

A coseismic decrease in water temperature by 0.008 °C for 7 min with a following recovery to the initial value was detected during the Sumatra M 9.1 2004 earthquake in a well 362 m deep located in the damage zone of a regional fault Huangzhuang-Gaoliying. The well tapped watered andesite tuff [4]. Temperature effects of one and the same type were also observed in this well during 25 earthquakes for the period of 2002–2005. A decrease in water temperature was traced for four earthquakes after the arrival of P-wave, but before the arrival of S-wave. For all the other earthquakes, noticeable variations in the water level and water temperature were observed after the arrival of S-wave.

Interval measurements of water temperature in 20 m steps were performed since 2007 at a depth of 20–240 m in the well K-1 located at the Kunashir Island of the West-Pacific seismic belt [5]. Increasing intensity of temperature oscillations with amplitudes of up to 0.2 °C and coseismic temperature effects, such as stepwise temperature rises were registered during the propagation of waves produced by earthquakes M 5.0–9.0 at epicentral distances 51–698 km [6].

The most representative data on coseismic and post-seismic hydrogeological effects were obtained in China during the Sichuan earthquake M 7.9 12 May 2008. Synchronous measurements of the water level and temperature were performed in 221 wells, only water temperature—in 45 wells, rock temperature—in 6 wells [7]. No unambiguous correspondence between variations in the water level and temperature were established.

Some authors [8–10] distinguish anomalous temperature effects in aquifers of different ages, which can be attributed to the period of earthquake preparation. Changes in the regime of thermal water three months before the catastrophic earthquake of Tohoku M 9.1 11 March 2011 at the distance of 155 km to the north-west from the epicenter in a well 2 km deep drilled in a seismically active fault and located nearby the Goyo Onsen hot spring, Japan, were detected via a retrospective analysis of in situ data [8]. The maximum water level decreased to 10 m. Water temperature episodically decreased by 1–2 °C.

It was established for one of the wells Yushu, China, 105 m deep, drilled in granites, that the intensity and duration of water temperature anomalies correlate with earthquake amplitudes and can be used as precursors [9]. Stepwise rises of temperature before the main shock and the main aftershock of the Sichuan earthquake M 7.9 12 May 2008 were traced in two wells 650 m and 99 m deep at the distances of 600 km and 1400 km from the epicenter, respectively [10]. An anomalous decrease in rock temperature by 0.002 °C was registered 18 days before the Sichuan earthquake in the well Xining (no. 63001) [7].

Disturbed hydrogeodynamical and hydrogeochemical regimes have formed inside regional and local areas subjected to anthropogenical load in the form of advanced mining industry [11–13]. Lowering of the level of underground water that can reach 40 m in the observation well at the distance of 100 m from the working face [14], and both gradual and

stepwise variations in water temperature with amplitudes of up to 0.45 °C [15] have been observed in the course of coal bed development.

In particular, before the mining operations started at the coal deposit Ningtiaota near the Ordos basin, China, the water temperature remained stable. As the front of tunneling approached the observation well J7 to the distance of 2 km on 8 January 2017, the water level lowered by 45 m and the temperature decreased stepwise by 0.45 °C with a delay of one day relative to the water level. Synchronous stepwise drops of the water level and temperature with amplitudes of 23 m and 0.3 °C, respectively, were observed on 5 January 2018 in the well J6 that tapped the aquifer roof 20 m higher in comparison to the well J7 at the distance of 1 km from the face [15].

In the well J14, which is 3.3–4.1 km away from observation wells J7 and J6, and located upstream, the general trend in a regional rise in the water level in the lower aquifer by 1.3 m during 2016–2018 is complicated by local depression cones with maximum level lowering by 0.6 m and temperature decrease of 0.2 °C, which lasted 2 days in 2017 and 1 day in 2018 when tunneling was performed beneath the observation wells. The observed peculiarities of the water level and temperature variations confirm the supposition of hydraulic links between the lower aquifer and the moving front of tunneling, despite the covering layers of argillite and siltstone 35–59 m thick lying above the coal seam.

The regime of underground water remains intact in the upper aquifer formed by sand rich sediments and separated from the lower aquifer by layers of clays, argillites and siltstone 80–120 m thick. An annual cyclicity has been established in variations in water temperature with the amplitude of 1.3 °C, which is synchronous to variations in atmospheric pressure with the amplitude of 0.2 kPa. These variations took place at the background of a regional rise in the groundwater level by 2 m for three years of observations [15].

Summarizing all above, the observed temperature effects that take place in natural and anthropogenically disturbed conditions were traced mainly in the low-frequency area during propagation of seismic waves originated from earthquakes, during earthquake preparation and during tunneling in deposits. The high-frequency response (15–20 Hz) of underground water to seismic impact produced by a ripple-fired explosion in a mine had already been instrumentally registered [16]. A question arises, whether similar temperature variations produced by a technogenic seismic impact on an aquifer can be detected in the high-frequency area? If “yes”, then whether such temperature effects can serve as signs of hydrogeodynamic processes that take place in the “reservoir–well” system?

Periodic observations over temperature in wells in aquifers of different ages are performed since 2021 within the framework of precise hydrogeological monitoring in the zones of mining lease of the iron ore deposits of the Kursk Magnetic Anomaly (KMA) [17]. The purpose of this research is to determine variations in the temperature, water level and filtration parameters of an aquifer produced by industrial explosions. Analyzing the coseismic changes in these parameters of the “reservoir–well” system can promote correct assess of the conditions of the rock massif, in which mining activities take place.

## **2. Brief Characteristics of Geological, Structural and Hydrogeological Conditions at the Site**

The region under investigation is located at the south-west slope of the Voronezh crystalline massif. Two structural floors were defined in the geological section. The lower floor is the crystalline basement, which is formed by complexly dislocated Precambrian metamorphosed rocks. It is complicated by discontinuities and intrusive formations [18].

The Korobkovskoye and Lebedinskoye iron ore deposits have complicated structures. They both are characterized by north-western strike of structures confined by faults of different ranks and directions. The faults manifest in the form of brecciation zones and zones of higher rock fracturing. The paleo-relief of the bed is a peneplain with eroded ridges of ferruginous quartzites. A line-pattern residual soil down to 100 m thick prevails on the crystalline rock.

The upper floor is the sedimentary cover folded mainly by terrigenous sedimentary deposits of Mezo-Cenozoic and covers transgressively the crystalline basement. Deposits of Paleozoic presented by the ore breccia and sandstones of the late Devonian 2–6 m thick show irregular bedding at the eroded cover of the Archaea-Proterozoic basement (Figure 1).

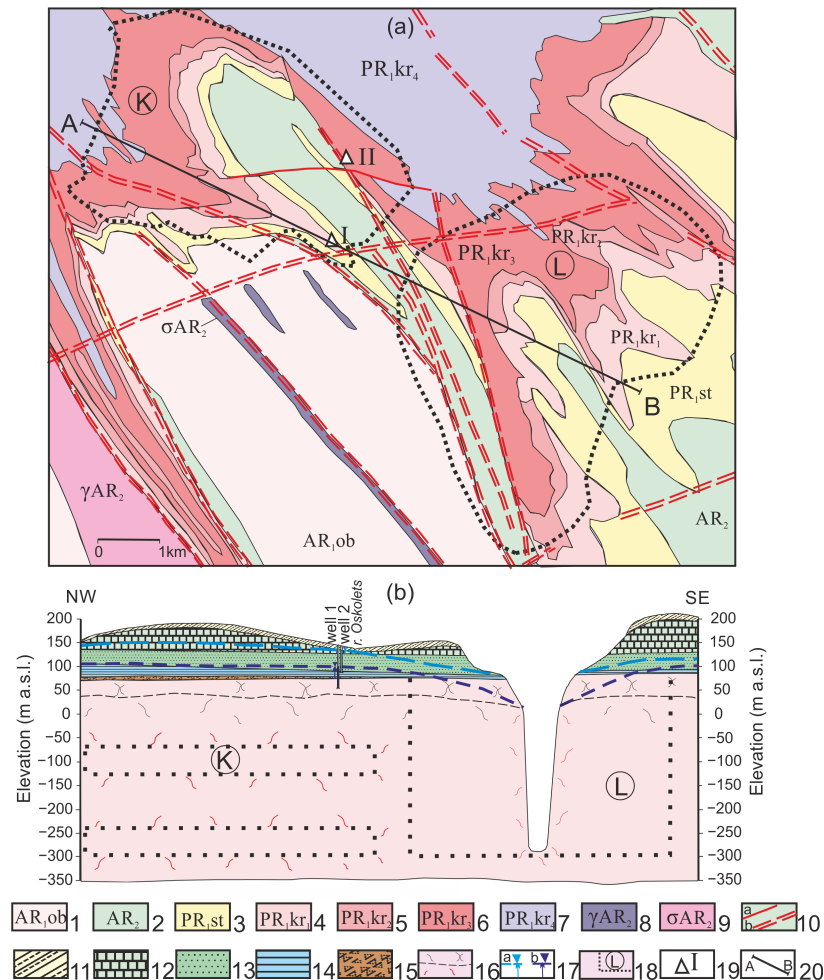


**Figure 1.** (a) Geological map of the basement of the region under investigation and (b) schematic geologic cross-section along the line A–B. Legend to the map (1–10): 1–9—formations: 1–2—Archean: 1—lower, 2—upper; 3–7—Lower Proterozoic: 3–7—Kursk series: 3—Stoilenskaya suite, 4–7—Korobkovskaya suite: 4, 6—lower and upper iron ore, 5, 7—intermediate; 8–9—intrusive formations of the Upper Archean; 10—faults: a—local, b—regional. (b) Legend to the cross-section (11–20): 11–15—sediments: 11—Cenozoic, 12—Upper Cretaceous, 13—Lower Cretaceous, 14—Upper Jurassic—Lower Cretaceous, 15—Upper-Middle Devonian, 16—Archean-Proterozoic (dashed line is the boundary between weathered and monolithic rock, black curves show petrogenetic fracturing, red curves are anthropogenic fracturing; 17—level of upper (a) and of lower aquifers (b); 18—boundaries of deposits (K—Korobkovskoe, L—Lebedinskoe), 19—observation points; 20—line of the cross-section.

Underground water of pore-seam type sedimentary deposits of Cretaceous (the upper Albian-Cenomanian confined aquifer) and fracture-seam type confined to the zone of exogenous erosion of rock in the crystalline bed (the lower Archaea-Proterozoic confined aquifer) mainly prevail at the site under investigation. The water of fracture-seam type feed the fracture-vein reservoirs widespread in the zones of high rock fracturing linked to faults and lithological contacts.

The regime of underground water is anthropogenically disturbed by the drainage systems that drain from the underground tunnels of the Korobkovskaya mine and the open



In order to assess the effect of atmospheric pressure on the level of underground water, the coefficient of barometric efficiency ( $BE$ ) is used, which is calculated as the ratio of underground water pressure ( $P_w$ ) to atmospheric pressure ( $P_b$ ):

$$BE = 1 - \frac{P_w}{P_b} \approx 1 - \frac{\Delta w}{\Delta b}. \quad (1)$$

The method of compensation based on the method of linear regression is used to “clean” the level of underground water from the effect of atmospheric pressure:

$$w' = w - A \cdot p, \quad A = \frac{\sum \Delta w \cdot \Delta p}{\sum \Delta p^2}, \quad (2)$$

where  $w'$  is the water level with pressure compensation (m),  $w$  is the water level (m),  $p$  is the atmospheric pressure ( $\text{kgf}/\text{m}^2$ ). Factor  $A$  is the ratio of the sum of the daily water level variation multiplied by daily variation in atmospheric pressure to the sum of quadratic daily pressure variation ( $\text{m}/(\text{kgf}/\text{m}^2)$ ).

Compressibility of the matrix is calculated according to [19]:

$$C_M = \frac{\theta_E C_W (1 - BE)}{BE} \quad (3)$$

where  $\theta_E$  is the rock effective porosity, which is 0.15 for sand rocks according to the literature [20],  $C_W$  is the fluid compressibility (compressibility of fresh water is  $C_W = 4.6 \times 10^{-10}$  Pa).

The theoretical ground displacement, vertical and cubic strains produced by Earth tides have been calculated for the point I using the ETERNA program [21]. In order to detect tidal waves in in situ (hydrogeological and barometric) and calculation data, filtration with a narrow band filter has been performed in the ranges 12.32–12.52 h and 25.7–25.9 h. The data were preliminarily decimated, and the sample rate reduced to 30 min.

In order to assess the phase shift  $\eta$  ( $^\circ$ ) between the tidal component in the water level and ground displacement, a method was used basing on calculation of delay of the sinusoid of tidal wave in the water level with respect to the sinusoid of tidal wave in ground displacement (using phase portraits) in coordinates “ground displacement—water level” [22]. The phase shift can be written as  $\eta = 2\pi t_p / \tau$ , where  $t_p$  is time delay of the peak of the water level with respect to the peak of the head,  $\tau$  is the wave period.

The semidiurnal wave of moon type  $M_2$  was chosen to determine filtration properties of fluid reservoir. The wave was detected in amplitude spectra of tides in the records of the water level in confined aquifer and in theoretical ground displacement. In quasi-stationary conditions, the horizon head traces ground displacement in the range of tidal waves in antiphase. Transmissivity  $T$  ( $\text{m}^2/\text{day}$ ) was calculated using the analytical solution [23]:

$$\eta = -\arctg \left( \frac{\frac{\omega r_c^2}{2T} \text{Ker}(\alpha_w)}{1 - \frac{\omega r_w^2}{2T} \text{Kei}(\alpha_w)} \right), \quad (4)$$

where  $\omega = 2\pi/\tau$  is the frequency of oscillations ( $\text{s}^{-1}$ ),  $\tau$  is the period of oscillations (s),  $r_c$  is the radius of casing (m),  $r_w$  is the radius of the well (m),  $\text{Ker}(\alpha_w)$  and  $\text{Kei}(\alpha_w)$  are the Kelvin functions of zero order,  $\alpha_w = (\omega S/T)^{1/2} \cdot r_w$ , and  $S$  is the elastic capacity of the formation.

The permeability of fluid reservoir  $k$  was estimated as follows:

$$k = \frac{\mu}{\rho g d} T, \quad (5)$$

where  $\mu$  is the coefficient of dynamic viscosity of formation,  $\rho$  is the water density ( $\text{kg}/\text{m}^3$ ),  $g$  is the acceleration of gravity ( $\text{m}/\text{s}^2$ ),  $d$  is the interval of watered segment of the well (m).

Iron ore deposits of the Kursk Magnetic Anomaly are being developed using blasting technologies. From 1 to 4 chambers are blasted during an industrial explosion in the mine at the Korobkovskoe deposit, from 1 to 7 groups—in the Lebedinsky quarry (each group consists of 1 to 4 blocks). They all are distributed in the depth interval from  $-315$  m to  $15$  m. In order to compare the experimental data, the maximum value of ground velocity  $V_m$  (hereinafter—mass velocity) is calculated in the observation point using three velocity components (one vertical  $V_Z$  and two horizontal ones  $V_N$  and  $V_E$ ) recorded during industrial explosions:

$$V_m = \left| \sqrt{V_Z^2 + V_N^2 + V_E^2} \right|. \quad (6)$$

The reduced distance is estimated as follows:

$$\bar{R} = \frac{R}{\sqrt[3]{Q}}, \quad (7)$$

where  $R$  is the epicentral distance from the center of the explosion to the observation point (m),  $Q$  is the maximum mass (kg) of explosive in one slowdown blasting set (or in one slowdown blasted block in the quarry).

The seismic energy density ( $\epsilon$ ) is calculated to compare the hydrogeological effects registered during industrial explosions [24]:

$$M = 2.7 + 0.69 \log \epsilon + 2.1 \log r, \quad (8)$$

where  $r$  is the epicentral distance (km),  $M$  is the magnitude estimated according to [25]

$$M(Y)_{max} = 2.45 + 0.73 \log Q, \quad (9)$$

where  $Q$  is the maximum mass (tons).

The seismic energy density is a universal parameter, because it combines two characteristics—the magnitude and the epicentral distance. The empirical relationship for earthquakes (8) was used to compare the results of seismic impacts on water reservoir, because there are no such relationships for industrial explosions so far.

#### 4. Results of Investigations

The results of hydrogeological monitoring being performed since 2019, are divided into two sections. The first section deals with the reaction of the “reservoir–well” system to quasi-static impacts (atmospheric pressure and Earth tides). This reaction may be treated as the background one. The second paragraph presents the results of registering the reaction to high-frequency impacts (industrial explosions in the neighboring mine and quarry).

##### 4.1. Monitoring the Permeability of Water-Saturated Reservoir

Seasonal variations in the water level in the upper aquifer (Figure 2) have been traced in the initial hydrogeological data for the period of observations of 2022–2023. Variations in the water level in the upper aquifer are asynchronous to variations in atmospheric pressure at low water (Figure 3a).

In the periods of spring–summer flood in 2022–2023, the correlation between the underground water level and atmospheric pressure is disturbed because of the changing feed conditions of aquifer and the rate of underground flow (Figure 3b). The coefficient of barometric efficiency was  $-0.50$  in 2022, and approximately  $-0.45$  in 2023 (Figure 3).

The obtained values of barometric efficiency were used to estimate the compressibility of the reservoir according to Equation (3). The compressibility of water-saturated rock manifests in pronounced season variations from  $3.5 \times 10^{-11}$  to  $2 \times 10^{-10}$  (Figure 4).

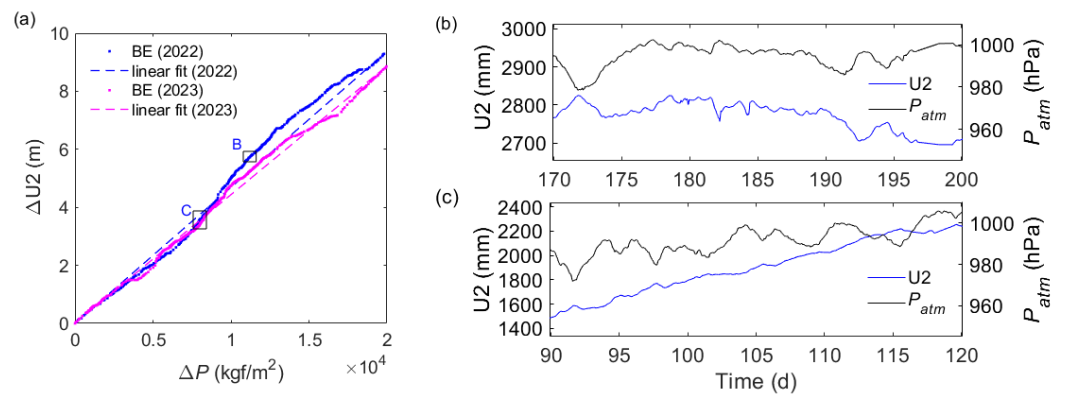


**Figure 3.** (a) Barometric efficiency and (b,c) variations in the underground water level (U2, blue line) and atmospheric pressure ( $P_{atm}$ , black line): (b)—asynchronous and (c)—disturbed.

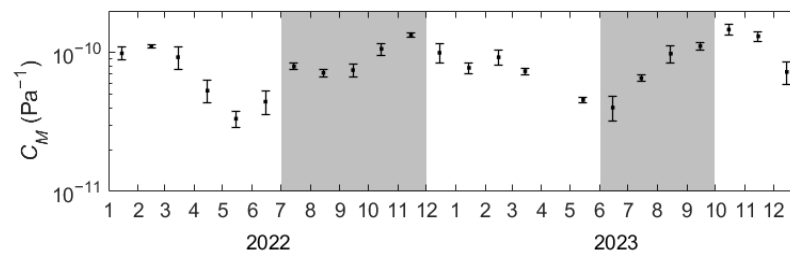


**Figure 4.** Compressibility of the water-saturated reservoir. Grey filling shows the intervals of the quasi-stationary filtration regime here and in Figures 5 and 6.

After the initial data were filtered from the effects of atmospheric pressure (Figure 5a), a decrease in piezometric surface was traced in the water level of the upper aquifer at the summer low water beginning from July 2022 and July 2023 (Figure 5b).

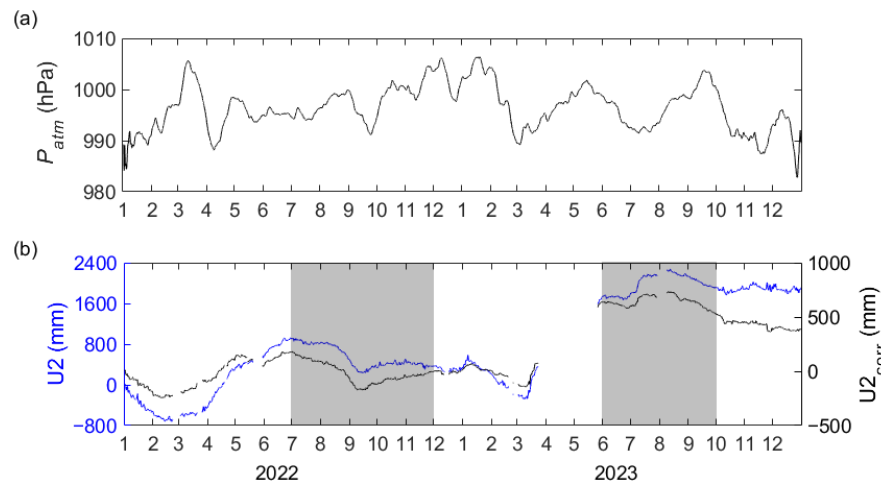


**Figure 5.** (a) Variations in atmospheric pressure; (b) relative water level in the upper aquifer (blue line) and cleared from the effect of atmospheric pressure (black line).

Annual variations in the head in the upper aquifer do not exceed 0.4–0.9 m. The periods of July–November 2022 and June–September 2023 show a quasi-stationary filtration regime, because the slopes of underground flow do not exceed 0.001–0.002. So, the data of these periods can be used to analyze the tidal sensitivity of water-saturated reservoir of the pore-seam type.

Three types of tidal waves were detected in the selected intervals: two semidiurnal waves (the sun  $S_2$  and the moon  $M_2$  types) and a diurnal wave of the sun-moon type ( $K_1$ ).

An estimation of filtration parameters of the water-saturated reservoir (transmissivity and permeability) has been performed basing on determination of the phase shift between the tidal wave  $M_2$  detected in theoretically calculated ground displacement and reaction of the water level in the upper aquifer according to Equations (4) and (5) (Figure 6). The 7-day intervals before and after the gaps in records, caused by technical reasons, were excluded from consideration, because the signal can be distorted at the “boundaries”.

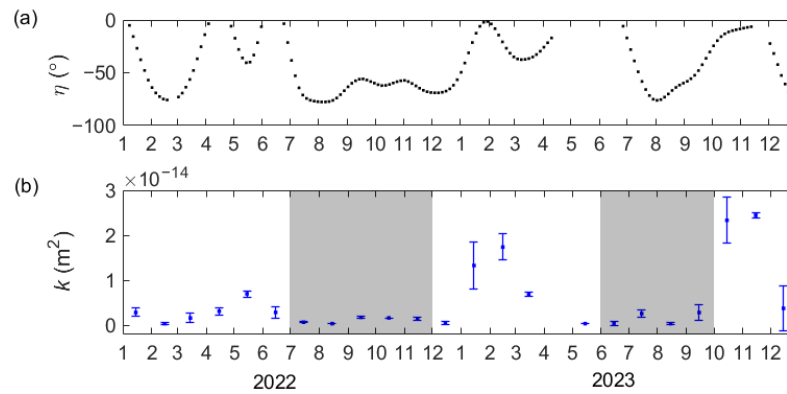


**Figure 6.** Variations in the (a) phase shift and (b) permeability of water-saturated reservoir.

According to the data recorded in 2022–2023, the transmissivity of the upper aquifer in the quasi-stationary filtration conditions vary from 0.015 to 0.035  $m^2/day$ . The permeability of the reservoir lies in the range of  $1.5 \times 10^{-15}$ – $2.7 \times 10^{-15} m^2$ . The water-saturated reservoir composed of uncemented sand sediments show weak permeability.

4.2. Variations in Temperature and Level of Underground Water under Seismic Impacts

For the 2.5 years of observations synchronous records of temperature and pressure in the upper aquifer were performed during 9 industrial explosions in chambers of the mine and during 30 explosions in the quarry.

No changes in temperature were fixed during seven explosions in the mine at reduced distances of 113–351  $m/kg^{1/3}$  and variations in pressure of 25–60 Pa, and during 11 explosions in the quarry. During 1 explosion in the mine and 14 explosions in the quarry, the reaction of the “reservoir–well” system did not exceed the accuracy of measurements, which is in the range of  $\pm 0.03 \text{ }^\circ\text{C}$ . Coseismic temperature changes were fixed during six industrial explosions (Table 1).

**Table 1.** Variations in water temperature and pressure in the “reservoir–well” system registered synchronously during industrial explosions.

Location of Industrial Explosions	№	Date	Water Temperature ( $^\circ\text{C}$ )			Pressure in the “Reservoir–Well” System (kPa)			Reduced Distance $\bar{R}$ ( $m/kg^{1/3}$ )	Mass Velocity $V_m$ (mm/s)
			min	max	$\Delta$	min	max	$\Delta$		
Coseismic responses:										
mine	1	30 October 2021	11.985	11.92	−0.065	−1.6	0.5	2.1	99	1.85
	2	14 September 2022	11.79	11.72	−0.07	20.89	22.52	1.63	114	7.79
	3	17 August 2022	11.79	11.73	−0.06	26.19	27.22	1.03	130.7	2.33
quarry	4	8 June 2022	11.84	11.93	0.09	25.52	27.67	2.15	131.4	5.79
	5	28 February 2024	11.44	11.50	0.065	39.14	39.54	0.40	204.0	1.47
	6	22 May 2024	11.52	11.58	0.06	44.36	45.97	1.61	118.1	4.91
Weak responses (in the range of sensor accuracy):										
mine	7	22 January 2022	11.981	12.025	0.044	14.3	14.8	0.5	127	1.62
	8	8 February 2023	11.76	11.71	−0.05	18.95	19.24	0.29	170.8	3.84
quarry	9	27 October 2021	11.96	11.92	−0.043	−1.0	0.9	1.90	185.6	3.61

Table 1. Cont.

Location of Industrial Explosions	№	Date	Water Temperature (°C)			Pressure in the “Reservoir–Well” System (kPa)			Reduced Distance $R$ (m/kg <sup>1/3</sup> )	Mass Velocity $V_m$ (mm/s)
			min	max	$\Delta$	min	max	$\Delta$		
quarry	10	13 September 2023	11.51	11.47	−0.04	38.81	39.58	0.77	175	2.76
	11	22 November 2023	11.39	11.35	−0.04	42.07	42.62	0.55	123	2.48
	12	7 December 2022	11.69	11.74	0.05	21.72	23.05	1.33	114.3	8.42
	13	28 December 2022	11.7	11.75	0.05	21.73	22.77	1.04	136.3	6.07
	14	12 July 2023	11.68	11.73	0.05	38.54	40.14	1.60	142	3.82
	15	19 June 2024	11.50	11.55	0.05	46.18	46.73	0.55	138.1	3.19
	16	10 April 2024	11.49	11.54	0.05	41.32	41.96	0.64	175	2.48
	17	8 December 2021	11.94	11.98	0.04	21.65	22.25	0.6	156.2	3.03
	18	8 May 2024	11.53	11.57	0.04	44.16	44.72	0.56	154	1.61
	19	16 February 2022	12.00	12.04	0.04	11.97	12.32	0.35	147.7	3.90
	20	29 June 2022	11.81	11.85	0.04	27.29	28.22	0.93	150.2	2.72
21	18 January 2023	11.72	11.76	0.04	21.77	22.59	0.82	183.8	3.99	

The effect of temperature decrease by 0.065 °C was fixed during the propagation of seismic waves produced by the explosion in the mine in a chamber located to the north-east from the observation point I down the underground flow at the reduced distance of 99 m/kg<sup>1/3</sup> (Figure 7) and during the propagation of seismic waves of two explosions in the western side of the quarry in the depth interval from −165 m to −45 m (Figure 8). Variations in pressure in the “reservoir–well” system were 1.0 kPa and 1.6 kPa, respectively.

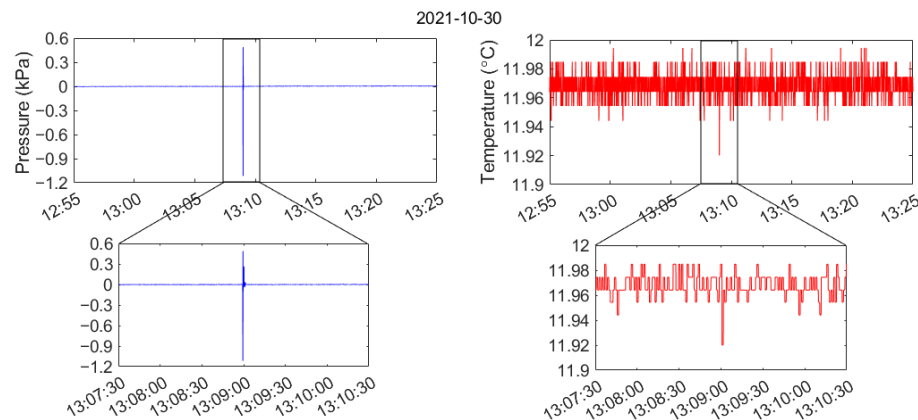


Figure 7. Variations in pore pressure and water temperature in the “reservoir–well” system during explosion 30 October 2021 in the mine.

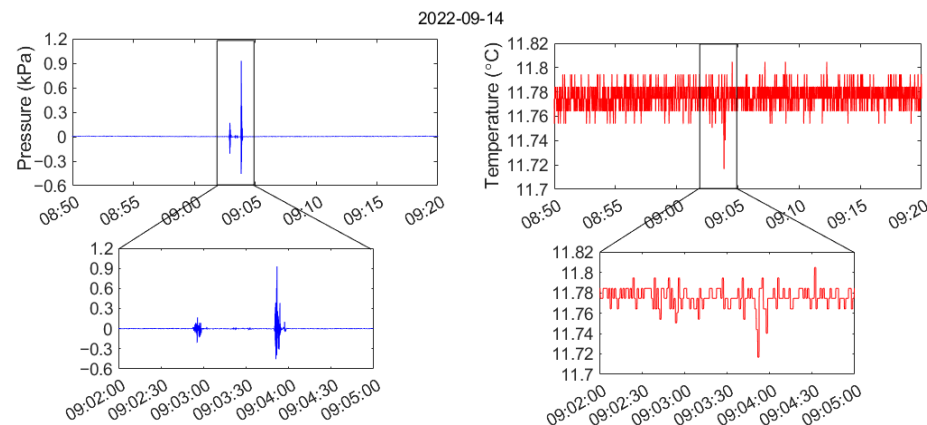
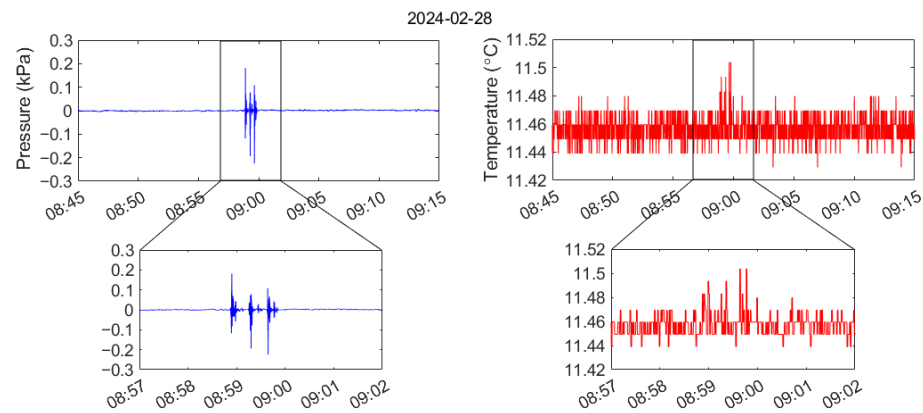


Figure 8. Variations in pore pressure and water temperature in the “reservoir–well” system during explosion 14 September 2022 in the quarry.

Water temperature increased in the aquifer by 0.06–0.09 °C during three industrial explosions in the western quarry side in the depth interval of –150 m to 15 m. The pressure in the “reservoir–well” system changed by 0.4–2.2 kPa (Figure 9).



**Figure 9.** Variations in pore pressure and water temperature in the “reservoir–well” system during the explosion 28 February 2024 in the quarry.

Thus, two types of coseismic effects were observed in processing the experimental data—water temperature increase and decrease, synchronous to the changes in pore pressure in the “reservoir–well” system. They all were observed during industrial explosions in the chambers of the mine and in the quarry. The relations between the reaction of the “reservoir–well” system and the parameters of industrial explosions show low coefficients of determination (Figure 10). The dependence of ground velocity on reduced distance is rather weak (Figure 10a). Values of ground velocity exceed the theoretical estimates made for explosions in the quarries of KMA [26]:

$$V_m = 2400 \left( \frac{Q^{1/3}}{R} \right)^{1.48} \quad (10)$$

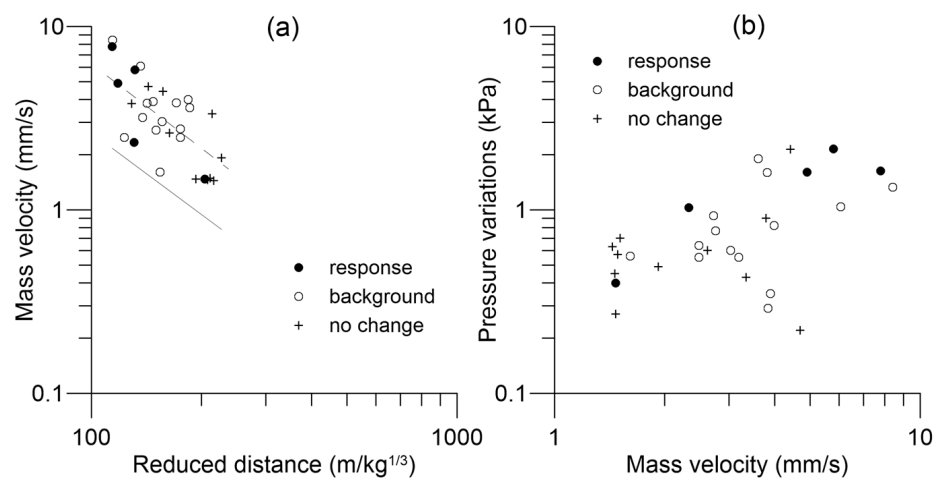


**Figure 10.** (a) Mass velocity ( $V_m$ ) versus reduced distance for industrial explosions in the quarry and (b) pore pressure in the “reservoir–well” system versus mass velocity (the legend of water temperature is given in accordance with Table 1. The solid line is calculated by Equation (10). The dashed line is calculated by Equation (11).

The empirical dependence of ground velocity on distance constructed via the data on industrial explosions in the quarry, for which simultaneously the water temperature in the upper aquifer was recorded, looks as follows:

$$V_m = 9618 \left( \frac{Q^{1/3}}{R} \right)^{1.59} . \tag{11}$$

An empirical dependence of variations in pore pressure in the “reservoir–well” system on ground velocity during industrial explosions has been traced (Figure 10a). Though the amplitudes of ground velocity are close, variations in pore pressure may differ by 1.5–3 times and even more, since the hydrogeological response of a water-saturated reservoir to seismic action depends not only on the parameters of explosion, but also on the local properties of the “reservoir–well” system.

An increase in the range of variations in the permeability of water-saturated reservoir for the entire period of observations and for the period of quasi-stationary conditions was traced in anthropogenically disturbed conditions as the head rose by 3.7 m in 2023 in comparison to 2022 (Figure 11a). The value of the median permeability of the reservoir in 2022 was  $1.5 \times 10^{-15} \text{ m}^2$ . It increased to  $2.7 \times 10^{-15} \text{ m}^2$  in 2023.

An inverse dependence was traced between the general trend in the decreasing water temperature and permeability of the reservoir (Figure 11b), which agrees with the change in temperature as the hydrostatic head increases (Figure 2b). In some cases, high values of coseismic response of temperature were observed as the permeability increased. A decrease in water temperature with increase in permeability probably occurs at the expense of inflow of colder water from the horizon to the “reservoir–well” system. The detected regularities testify changes in filtration properties of water-saturated rock.

Taking into account the scheme that shows the location of observation point I with respect to the sites where explosions in the quarry were performed it should be noted that coseismic changes in temperature took place in blasting the blocks that are located mainly along the western side of the quarry (Figure 12). Judging by the cross-section presented in Figure 1b, it is this zone that the drained series of the fracture-seam type and fracture-vein type are located in.

The reaction of the “reservoir–well” system to industrial explosions on the boarder of accuracy of measurements was observed mainly during industrial explosions in the center of the quarry and along its eastern side in the depth interval of  $-315 \text{ m}$  to  $-45 \text{ m}$ .

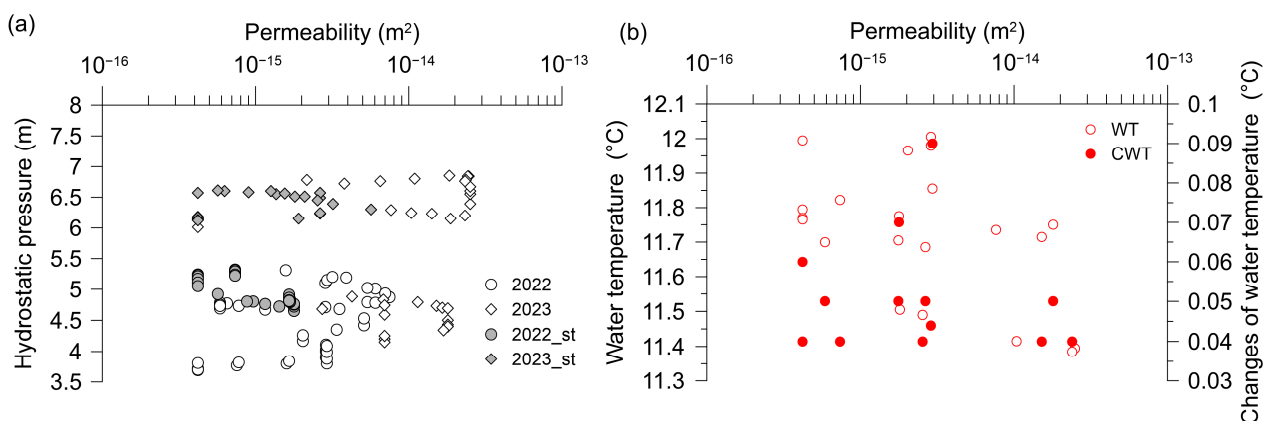


**Figure 11.** (a) Permeability of water-saturated reservoir versus hydrostatic pressure. (b) Water temperature (WT) and coseismic response of water temperature (CWT) in the upper aquifer versus permeability (legend for water temperature is given in accordance with Table 1. Index “st” denotes the periods of quasi-stationary filtration).

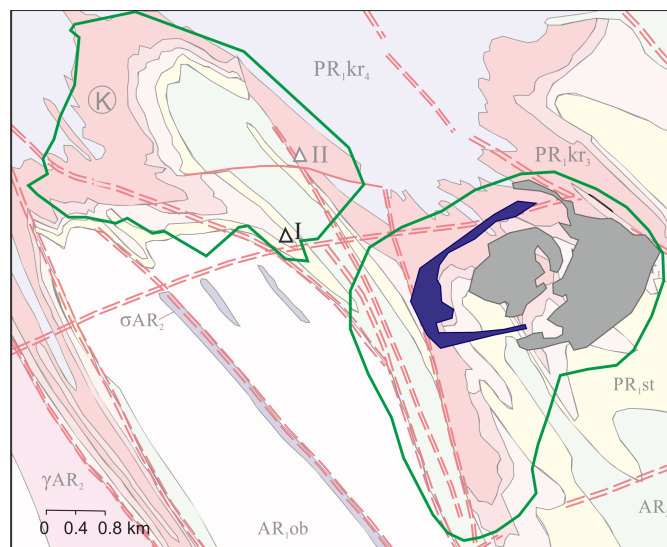


**Figure 12.** Location of blocks blasted in the quarry, for which water temperature in the upper aquifer was registered at point I. Blue color denotes blocks, for which coseismic temperature effects were detected. Grey color denotes blocks, for which the results lie in the range of sensor accuracy limits. Green color denotes the contours of the mine and quarry sites.

## 5. Discussion

Different mechanisms are considered in analyzing factors that impact on coseismic and post-seismic changes in water temperature produced by passing seismic waves of earthquakes and tunneling. One of the main mechanisms that determines the coseismic temperature effects is the change in the permeability of a water-saturated reservoir under seismic impact.

Let us give examples. Two earthquakes Lijiang M 7.0 3 February 1996 and Sumatra M 9.1 26 December 2004 produced stepwise decreases in water discharge by 0.001–0.003 L/s and in temperature by 2.5–4 °C in the thermal spring Banglazhang #1 (China), which is fed through the Xiangbaihe fault zone. These coseismic changes were observed at the background of the decreasing permeability of the fault zone. The disturbed parameters recovered to the initial values in half a year [27].

On the contrary, at the expense of increasing the permeability of water-saturated rock under seismic impact and increasing the discharge of underground water, a decrease in water temperature can take place together with a lowering water level in the observation well. This case was observed in the wells located along the Chelungpu fault according to the data of episodic measurements performed before and after the intraplate earthquake Chi-Chi M 7.3 21 September 1999 [28]. On the other hand, coseismic temperature effects can be linked to convection processes on account of oscillations in the water level during the propagation of seismic waves of earthquakes [4].

The mechanism that underlies such effects can be as follows. A synchronous rise in the water level, an increase in discharge and in temperature can be accounted for by an increase in the permeability of the aquifer caused by an earthquake and by the mechanism of mixing water with adjacent aquifers with higher heads [3] and different water temperatures (higher or lower than the one in the aquifer under investigation) [7]. Presence of a thermal spring (as in the abovementioned case) can reverse the effect.

In a seismically active region, manifestation of temperature anomalies probably testifies a tectonic activation of the region. In particular, the registered variation in water temperature in the well Yushu, China before earthquakes may be caused by regional tectonics, as the Indian plate obducts over the Tibetan block [10].

For anthropogenically disturbed conditions, the maximum drop in the water level and temperature was observed during tunneling under the wells J7 and J6 with a one-

year gap. The effect was probably caused by emerging vertical and horizontal fractures. The following recovery of level and temperature was probably promoted by clogging of the hydrologically active fractures as the face of tunneling moved forward and the hydrostatic pressure rose. The results of processing in situ data presented in [15] show that the elastic capacity of watered rock lowers from  $3 \times 10^{-5}$  to  $0.5 \times 10^{-7}$  as the front of tunneling approaches the wells J7 and J6 to the distance of 400 m and 230 m, respectively, and probably the inflow of fresh underground water determines the stepwise drop of temperature.

Comparing variations in water temperatures registered during earthquakes worldwide and industrial explosions at KMA, it should be noted that the coseismic response of temperature occurs mainly when the seismic energy densities of earthquakes and explosions are of close values and lie in the range of 0.005–0.96 J/m<sup>3</sup> (Figure 13). Hence, if the intensities of seismic impacts of an earthquake and an explosion are comparable, the mechanisms that determine the deformation regime of water-saturated reservoirs may be similar.

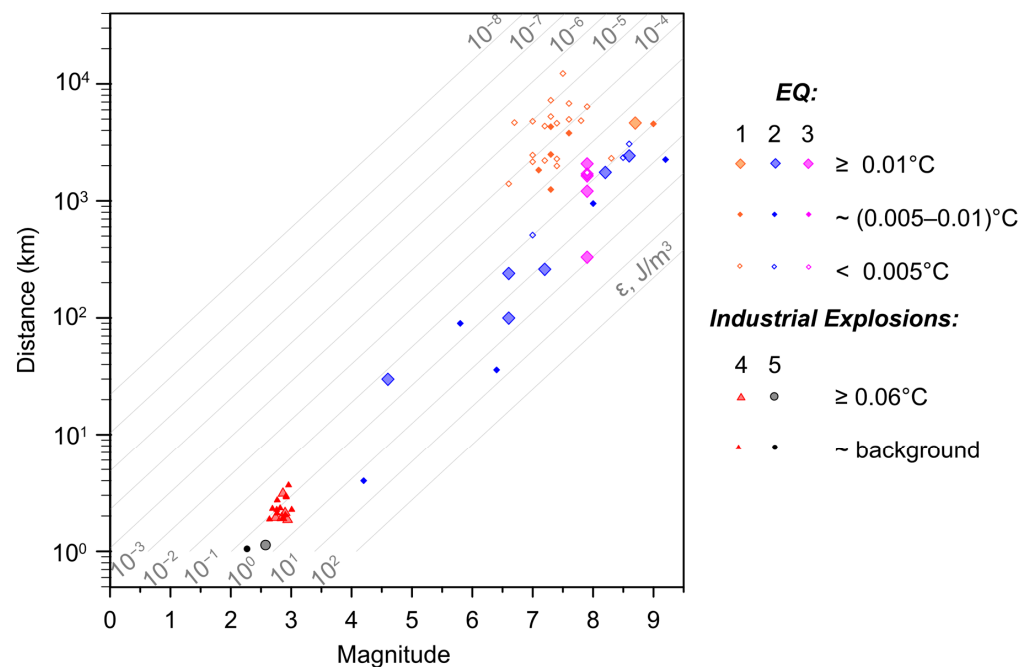


**Figure 13.** Distance–magnitude dependence for earthquakes (EQ) and industrial explosions at KMA. The diagonal grid shows variations in seismic energy density. The legend gives corresponding data on water temperature measurements in aquifers (coseismic and post-seismic changes) (1—Yang et al., 2007 [4]; 2—Zhang et al., 2023 [3]; 3—He, Singh, 2020 [7]; 4—mine; 5—quarry).

The model that explains dynamic deformation of a water-saturated reservoir is based on the theory of poroelasticity. The deformation can occur either via changes in the stress–strain conditions of the “matrix” (deformation of the rock skeleton of the massif), or via changes in pore pressure in the reservoir propagating through water. In most cases, both mechanisms compete and can lead to oscillations in the water level and temperature [2,29]. No unambiguous correspondence was observed between hydrogeological and temperature effects under seismic impacts. Hence, a more complicated model can be considered, which, for example, should take into account the presence of colloidal micro-particles in water and the processes of the pores clogging/unclogging under varying pore pressure [30].

The regime of the upper aquifer in the anthropogenically disturbed conditions of KMA depends on different factors: regional trend in the hydrostatic head, seasonal variations in the compressibility and permeability of a water-saturated reservoir and intensity of seismic impact on the “reservoir–well” system. The coseismic changes in water temperature of

$\pm 0.06$ – $0.09$  °C have mainly been registered during propagation of seismic waves performed in the western side of the quarry, conjugate to the filtration structure of the rock massif being developed.

The poroelastic response of a water-saturated reservoir of sand sediments to seismic impact is clearly manifested in pore pressure oscillations with an amplitude of up to 1.9 kPa and can lead to the “activation” of colloidal microparticles. Diverse changes in temperature in the “reservoir–well” system during propagation of seismic waves from industrial explosions during the development of iron ore deposits of KMA are probably caused by the skin effect—local change in permeability in the near-well zone.

A short-term increase in water temperature under seismic impact can originate from an episodic pore clogging and manifests mainly during the quasi-stationary filtration regime.

On the contrary, a decrease in water temperature may be caused by declogging and an increase in permeability that determines the intensity of water inflow into the “reservoir–well” system from the aquifer. The considered mechanism is consistent with the model of changing permeability caused by clogging/unclogging of micro-cracks in rocks which manifests in coseismic and post-seismic variations in the underground water level during earthquakes [31]. Clogging of micro-cracks may lead to a decrease in permeability, an increase in pore pressure and in temperature in the “reservoir–well” system. The opposite effect of declogging facilitates an increase in permeability and additional inflow of “colder” water from the aquifer. The results of laboratory experiments, performed under seismic impacts of different intensities, confirm the possibility of emerging micro-barriers and their destruction [32].

Thus, the temperature of underground water is also one of the main indicators of changes in the permeability of water reservoirs. Of great importance is obtaining representative series of synchronously registered temperature and pore pressure in the “reservoir–well” system in the course of developing mineral deposits. The data of water temperature monitoring can be used to control the dynamics of a water-saturated reservoir deformation under quasi-stationary and episodic effects.

## 6. Conclusions

For the period of observations 2021–2024, the following results were obtained:

- Variations in water temperature and level have been determined in the upper aquifer taped in the interval of 14.5–53.5 m (this interval is confined to sand sediments of early Cretaceous).
- The trend in lowering water temperature has been traced from 12 °C to 11.4 °C as the underground water level showed a regional rise from 10.8 m to 7.6 m. The gradient of temperature decrease in the upper aquifer is 0.19 °C/m.
- The detected pattern indicates that natural resources of underground water gradually recover in the area of the iron ore deposits of KMA.

A synchronous recording of water temperature and pore pressure in the “reservoir–well” system was performed during 9 industrial explosions in the mine chambers and during 30 quarry explosions. In three cases, the effect of increasing water temperature during the propagation of seismic waves of industrial explosions in the quarry by 0.06–0.09 °C was observed. A decrease in water temperature by 0.06–0.07 °C was observed during an explosion in the mine chamber at reduced distance of 99 m/kg<sup>1/3</sup> and two explosions in the quarry. Coseismic changes in water temperature were detected, but did not exceed sensor accuracy for 14 explosions in the quarry (they were performed mainly in its center and at its eastern side, in the depth interval of –315 m to 15 m) and for 1 explosion in the mine. During the rest of the 18 explosions, no changes in water temperature were registered.

The coseismic responses of water temperature in the upper aquifer were observed mainly when the blocks at the western side of the quarry were blasted, closest to the observation point I, with a relatively shallow position of the blocks in the depth interval of –165 m to –45 m. Short-term changes in water temperature in the “reservoir–well” system

can be accounted for by the skin effect—local changes in permeability in the near-well zone. An increase in water temperature is probably produced by a short-term clogging of the pores by the colloidal micro-particles during the propagation of seismic waves of industrial explosions. And on the contrary, declogging of the pores due to water inflow into the “reservoir–well” system facilitates water temperature decrease.

Coseismic (and more rarely—post-seismic) variations in temperature in aquifers were observed during earthquakes in seismically active regions. Similar effects produced by seismic waves were observed during industrial explosions at KMA. It is essential that for both sources (earthquakes and explosions), the temperature variations were recorded only when the seismic energy density was in the range of 0.005–0.96 J/m<sup>3</sup>.

A continuation of studies of the observed regularities of variations in the temperature of aquifers located close to the front of tunneling provides perspective because it promotes understanding the hydrogeodynamical and hydrogeomechanical processes that take place in mining activities.

**Author Contributions:** Conceptualization, E.G.; formal analysis, E.G., S.P. and A.I.; investigation, Z.S., A.K. and A.F.; methodology, E.G., S.P. and Z.S.; project administration, E.G.; software, S.P. and A.I.; writing—original draft, E.G., S.P. and D.P.; writing—review and editing, E.G., S.P. and D.P. All authors have read and agreed to the published version of the manuscript.

**Funding:** This research was funded by the Russian Science Foundation, project No. 23-27-00469. <https://rscf.ru/project/23-27-00469/> (accessed on 28 August 2024).

**Data Availability Statement:** The data presented in this study are available on request from the corresponding author (the data are not publicly available due to privacy).

**Acknowledgments:** We are grateful to Alina Besedina for valuable advices and notes during the preparation of the article and to anonymous reviewers for their useful commentaries.

**Conflicts of Interest:** The authors declare no conflicts of interest.

## References

- Chen, S.; Liu, P.; Guo, Y.; Liu, L.; Ma, J. Co-Seismic Response of Bedrock Temperature to the Ms6.3 Kangding Earthquake on 22 November 2014 in Sichuan, China. *Pure Appl. Geophys.* **2019**, *176*, 97–117. [[CrossRef](#)]
- Wang, C.-Y.; Manga, M. *Water and Earthquakes*; Springer Nature: Berkeley, CA, USA, 2021; 386p. [[CrossRef](#)]
- Zhang, S.; Shi, Z.; Wang, G.; Zhang, Z.; Guo, H. The Origin of Hydrological Responses Following Earthquakes in a Confined Aquifer: Insight from Water Level, Flow Rate, and Temperature Observations. *Hydrol. Earth Syst. Sci.* **2023**, *27*, 401–415. [[CrossRef](#)]
- Yang, Z.; Deng, Z.; Tao, J.; Gu, Y.; Wang, Z.; Liu, C. Coseismic Effects of Water Temperature Based on Digital Observation from Tayuan Well, Beijing. *Acta Seismol. Sin. Engl. Ed.* **2007**, *20*, 212–223. [[CrossRef](#)]
- Yurkov, A.K.; Demezhko, D.Y.; Outkin, V.I. On the informativeness of temperature monitoring measurements in wells when studying the tectonic regime. *Bull. Natl. Nucl. Cent. Repub. Kazakhstan* **2012**, *2*, 93–95. (In Russian)
- Yurkov, A.K.; Demezhko, D.Y. On the issue of quasi-periodic temperature oscillations in the KUN-1 well (Kunashir Island). In *Geodynamical Processes and Natural Hazards, Proceedings of the International Scientific Conference, Yuzhno-Sakhalinsk, Russia, 26–30 May 2015*; Dalnauka: Vladivostok, Russia, 2015; Volume 1, pp. 294–297. (In Russian)
- He, A.; Singh, R.P. Coseismic Groundwater Temperature Response Associated with the Wenchuan Earthquake. *Pure Appl. Geophys.* **2020**, *177*, 109–120. [[CrossRef](#)]
- Orihara, Y.; Kamogawa, M.; Nagao, T. Preseismic Changes of the Level and Temperature of Confined Groundwater Related to the 2011 Tohoku Earthquake. *Sci. Rep.* **2014**, *4*, 6907. [[CrossRef](#)]
- Sun, X.; Xiang, Y.; Shi, Z.; Wang, B. Preseismic Changes of Water Temperature in the Yushu Well, Western China. *Pure Appl. Geophys.* **2018**, *175*, 2445–2458. [[CrossRef](#)]
- Huang, F.; Yuchuan, M. The Temperature Changes before and after the 2008 Wenchuan Earthquake and Their Implication to Continental Tectonic and Earthquake Process. In *Proceedings of the CGS/SEG International Geophysical Conference, Qingdao, China, 17–20 April 2017*; Society of Exploration Geophysicists and Chinese Petroleum Society: Beijing, China, 2017; pp. 1297–1299. [[CrossRef](#)]
- Mironenko, V.A.; Molsky, E.V.; Rumynin, V.G. *Mining and Industrial Hydrogeology*; Nedra: Moscow, Russia, 1989; 287p. (In Russian)
- Zhitinskaya, O.M. Influence of Components of Engineering-Geological Conditions on the Stability of the Slopes of Iron Ore Quarries during Their Long-Term Development. Ph.D. Thesis, Geological and Mineralogical Sciences, Moscow, Russia, 2018; 145p. (In Russian)
- Rybnikova, L.S.; Navolokina, V.Y. Assessment of the hydrosphere state of the upper reaches of the Tagil River basin (Sverdlovsk region). *Probl. Subsoil Use* **2020**, *2*, 81–89. (In Russian) [[CrossRef](#)]

14. Norvatov, Y.A. *Study and Forecast of the Technogenic Regime of Underground Waters (during the Development of Mineral Deposits)*; Nedra: Leningrad, Russia, 1988; 261p. (In Russian)
15. Qu, S.; Wang, G.; Zhang, S.; Shi, Z.; Liang, X.; Luo, A. Deciphering the Mechanism of Groundwater Temperature Changes Associated with Longwall Mining in a Coalfield, China, Using the Extreme Gradient Boosting Method. *Hydrogeol. J.* **2024**, *32*, 1419–1432. [[CrossRef](#)]
16. Pavlov, D.V.; Besedina, A.N.; Gorbunova, E.M.; Ostapchuk, A.A. Response of an aquifer to the passage of seismic waves in the close-in zone of a ripple-fired explosion in a mine. In Proceedings of the ISRM International Symposium—EUROCK 2020, Hard Rock Engineering, Trondheim, Norway, 14–19 June 2020; ISRM-EUROCK-2020-166; Li, C.C., Ødegaard, H., Høien, A.H., Macias, J., Eds.; OnePetro: Richardson, TX, USA, 2020; ISBN 978-82-8208-072-9.
17. Gorbunova, E.; Besedina, A.; Petukhova, S.; Pavlov, D. Reaction of the Underground Water to Seismic Impact from Industrial Explosions. *Water* **2023**, *15*, 1358. [[CrossRef](#)]
18. Golivkin, N.I.; Kononov, N.F.; Orlov, V.P. *Iron Ores of KMA*; Geoinformmark: Moscow, Russia, 2001; 616p. (In Russian)
19. Turnadge, C.; Crosbie, R.S.; Barron, O.; Rau, G.C. Comparing Methods of Barometric Efficiency Characterization for Specific Storage Estimation. *Groundwater* **2019**, *57*, 844–859. [[CrossRef](#)] [[PubMed](#)]
20. Khanin, A.A. *Oil and Gas Reservoir Rocks and Their Study*; Nedra: Moscow, Russia, 1969; 368p. (In Russian)
21. Wenzel, H.G. The NanoGal software: Earth Tide Data Processing Package ETERNA 3.30. *Bull. Inf. Marées Terrestres.* **1996**, *124*, 9425–9439.
22. Kabychenko, N.V. Evaluation of the phase shift between tidal deformation and variations in the water level in the well. In *Local and Global Manifestations of Impacts on the Geosphere: Collection of Scientific Papers of IDG RAS*; GEOS: Moscow, Russia, 2008; p. 6272. (In Russian)
23. Hsieh, P.A.; Bredehoeft, J.D.; Farr, J.M. Determination of Aquifer Transmissivity from Earth Tide Analysis. *Water Resour. Res.* **1987**, *23*, 1824–1832. [[CrossRef](#)]
24. Wang, C.-Y. Liquefaction beyond the Near Field. *Seismol. Res. Lett.* **2007**, *78*, 512–517. [[CrossRef](#)]
25. Khalturin, V.I.; Rautian, T.G.; Richards, P.G. The Seismic Signal Strength of Chemical Explosions. *Bull. Seismol. Soc. Am.* **1998**, *88*, 1511–1524. [[CrossRef](#)]
26. Kocharyan, G.G.; Kulikov, V.I.; Pavlov, D.V. Impact of Massive Blasts on Stability of Tectonic Faults. *J. Min. Sci.* **2019**, *55*, 905–913. [[CrossRef](#)]
27. Yan, X.; Shi, Z.; Zhou, P.; Zhang, H.; Wang, G. Modeling Earthquake-Induced Spring Discharge and Temperature Changes in a Fault Zone Hydrothermal System. *J. Geophys. Res. Solid Earth* **2020**, *125*, e2020JB019344. [[CrossRef](#)]
28. Wang, C.-Y.; Manga, M.; Wang, C.H.; Chen, C.H. Transient Change in Groundwater Temperature after Earthquakes. *Geology* **2012**, *40*, 119–122. [[CrossRef](#)]
29. Kopylova, G.N.; Boldina, S.V. Effects of Seismic Waves in Water Level Changes in a Well: Empirical Data and Models. *Izv. Phys. Solid Earth* **2020**, *56*, 530–549. [[CrossRef](#)]
30. Petukhova, S.M.; Gorbunova, E.M. Deformation regimes of fluid-saturated reservoirs under seismic impact according to precision hydrogeological monitoring data (a review). *Dyn. Process. Geosph.* **2024**, *15*, 44–59. (In Russian) [[CrossRef](#)]
31. Brodsky, E.E.; Roeloffs, E.; Woodcock, D.; Gall, I.; Manga, M. A mechanism for sustained groundwater pressure changes induced by distant earthquakes. *J. Geophys. Res.* **2003**, *108*, 7-1–7-10. [[CrossRef](#)]
32. Kocharyan, G.G.; Vinogradov, E.A.; Gorbunova, E.M.; Markov, V.K.; Markov, D.V.; Pernik, L.M. Hydrologic Response of Underground. *Izv. Phys. Solid Earth* **2011**, *47*, 1071–1082. [[CrossRef](#)]

**Disclaimer/Publisher’s Note:** The statements, opinions and data contained in all publications are solely those of the individual author(s) and contributor(s) and not of MDPI and/or the editor(s). MDPI and/or the editor(s) disclaim responsibility for any injury to people or property resulting from any ideas, methods, instructions or products referred to in the content.